



In vivo localization of cortical areas using a 3D computerized atlas of the marmoset brain

Laurent Risser¹ · Amirouche Sadoun² · Muriel Mescam² · Kuzma Strelnikov² · Sandra Lebreton¹ · Samuel Boucher² · Pascal Girard^{2,3} · Nathalie Vayssière² · Marcello G. P. Rosa^{4,5} · Caroline Fonta²

Received: 2 August 2018 / Accepted: 25 March 2019
© Springer-Verlag GmbH Germany, part of Springer Nature 2019

Abstract

We created a volumetric template of the marmoset (*Callithrix jacchus*) brain, which enables localization of the cortical areas defined in the Paxinos et al. (The marmoset brain in stereotaxic coordinates. Elsevier Academic Press, Cambridge, 2012) marmoset brain atlas, as well as seven broader cortical regions (occipital, temporal, parietal, prefrontal, motor, limbic, insular), different brain compartments (white matter, gray matter, cerebro-spinal fluid including ventricular spaces), and various other structures (brain stem, cerebellum, olfactory bulb, hippocampus). The template was designed from T_1 -weighted MR images acquired using a 3 T MRI scanner. It was based on a single fully segmented marmoset brain image, which was transported onto the mean of 13 adult marmoset brain images using a diffeomorphic strategy that fully preserves the brain topology. In addition, we offer an automatic segmentation pipeline which fully exploits the proposed template. The segmentation pipeline was quantitatively assessed by comparing the results of manual and automated segmentations. An associated program, written in Python, can be used from a command-line interface, or used interactively as a module of the 3DSlicer software. This program can be applied to the analysis of multimodal images, to map specific cortical areas in lesions or to define the seeds for further tractography analyses.

Keywords MRI · New world monkey · Mapping · Template · Cortex

Introduction

The brains of non-human primates (NHP) show important neuroanatomical similarities with the human brain, particularly in terms of the composition of cortical areas. These structural homologies, which are less obvious in other species of mammal commonly used in laboratories (e.g., rodents), translate into neurophysiological and cognitive characteristics which are essential in animal models to

explore mechanisms of human normal and abnormal behavior (see, e.g., Mansouri et al. 2017).

The common marmoset (*Callithrix jacchus*) is a new world monkey which is being increasingly used in a large variety of studies, and more specifically in neuroscience (Marx 2016; Miller et al. 2016; Mitchell and Leopold 2015; Okano and Mitra 2015; Okano et al. 2016; Prins et al. 2017). Relative to the more commonly used old world macaque monkeys, marmosets offer advantages related to their small sizes, relatively rapid reproductive cycle, development and maturation, and the fact that the genome has been fully mapped, which facilitates the production of transgenic lineages (Marmoset Genome Sequencing and Analysis Consortium 2014; Sasaki 2015; Tomioka et al. 2017). They share fundamental features of brain architecture with humans (Bakola et al. 2015; Ghahremani et al. 2016; Hashikawa et al. 2015; Paxinos et al. 2012; Solomon and Rosa 2014) and specific cognitive functions (Burkart and Finkenwirth 2015; Nummela et al. 2017; Spinelli et al. 2004; Takemoto et al. 2015). Moreover, the marmoset brain has a lissencephalic cortex, which shows relatively little individual

Laurent Risser, Amirouche Sadoun and Muriel Mescam have equal contribution.

Electronic supplementary material The online version of this article (<https://doi.org/10.1007/s00429-019-01869-x>) contains supplementary material, which is available to authorized users.

✉ Marcello G. P. Rosa
marcello.rosa@monash.edu

✉ Caroline Fonta
caroline.fonta@cnrs.fr

Extended author information available on the last page of the article

anatomical variability. This greatly simplifies the implementation of imaging and computational methodologies (Majka et al. 2016) and also facilitates the longitudinal study of cohorts of individuals using non-invasive imaging techniques (Sawiak et al. 2018). Such longitudinal studies can provide a direct basis of comparison with human studies that use the same techniques (Amlien et al. 2016). In addition, preliminary routine brain imaging is also useful for ensuring lack of brain anomalies in animals destined for other types of investigations (Sadoun et al. 2015; Tu et al. 2014). Thus, NMR-based techniques (MRI, fMRI, MR spectroscopy) and molecular imaging (SPECT, PET) methods are being developed to provide data on the marmoset brain anatomy and metabolic activity, including the structure of the tissue and the distribution of neurochemicals (Belcher et al. 2016; Bock et al. 2009; Converse et al. 2012; Garea-Rodriguez et al. 2012; Meyer et al. 2006; Silva 2017; Yokoyama et al. 2010).

The creation of marmoset brain atlases over the last decade has been an important enabling step, which in turn makes possible studies involving the detection of anatomical changes in specific structures, as well as the localization of functional processes and biochemical properties. Several atlases of the marmoset brain have been published based on histology (Palazzi and Bordier 2008; Paxinos et al. 2012; Senoo et al. 2015; Stephan et al. 1980), and three atlases have used a combination of histology and MRI (Newman et al. 2009; Woodward et al. 2018; Yuasa et al. 2010). Several of the previous atlases only provide a very coarse subdivision of the cortex, using landmarks such as sulci, which are not generally sufficient to reliably identify cortical areas. This limitation is particularly important when considering regions such as the frontal cortex, where many small areas are present in a complex mosaic (Bakola et al. 2015; Burman et al. 2006, 2007; Fuster 2001; Preuss and Goldman-Rakic 1991; Yeterian et al. 2012). Because such cortical areas contribute to many of the high-order cognitive processes that are key to the evolutionary process of primate brains (Fuster 2002; Gebhard et al. 1995; Mansouri et al. 2017; Suzuki et al. 2015), defining their location and variability is essential.

The marmoset cerebral cortex has been analyzed using neurochemical markers, connectivity tracers, electrophysiological recordings and functional MRI (e.g. (Bourne and Rosa 2006; Burman et al. 2006, 2011, 2014, 2015; Krubitzer and Kaas 1990; Lui et al. 2006; Toarmino et al. 2017), and (Majka et al. 2016; Paxinos et al. 2012) for summaries). This offers the possibility to localize cortical areas on marmoset MRI-imaged brains to provide a '3D cortical area atlas' (Hashikawa et al. 2015; Woodward et al. 2018). Here, we provide a new template of the marmoset brain with a representation of the cortical areas and segmentations of brain structures. This template (which, to distinguish from others, we will refer to as the IMPEC template, from the name of

the CerCo team that initiated the work) is obtained by a semi-automatic segmentation of an adult marmoset brain imaged with a clinical 3 T magnet. To represent an average template, the original segmented marmoset brain image and its segmentations were transported to the Karcher mean of representative marmoset brain images using the diffeomorphic framework of (Fiot et al. 2014; Vialard et al. 2012b). The resulting average template can then be considered as the center of gravity of the representative brain images, as detailed in (Fiot et al. 2014; Vialard et al. 2012b).

We additionally describe a user-friendly tool for the semi-automatic registration of brain regions and cortical areas on any marmoset brain MRI, based on our template and on the atlas from (Paxinos et al. 2012). These registration results can serve for segmentation purpose. This tool was developed in Python with SimpleITK (<http://www.simpleitk.org/>) and can either be launched using command lines or as a fully integrated module for the program Slicer (Fedorov et al. 2012). The IMPEC marmoset brain template and the segmentation pipeline in Python are freely available on sourceforge at the address <https://sourceforge.net/projects/impecbrainseg/>.

Methods

Subjects

Male and female adult marmoset monkeys (*C. jacchus*) were bred in CerCo (agreement B31 555 01 from Haute Garonne Prefecture, France). All experimental procedures were conform to Directive 2010/63/EU and were carried out according to the National Committee for Ethical Reflection on Animal Testing. The project received the regional (MP/03/76/11/12) and the governmental authorizations from the MENESR (project 05215.03).

Animals were housed in pairs or small groups and maintained in a 12:12 h light–dark cycle. Food and water were withdrawn from the cages in the morning preceding the imaging session. All imaging sessions were conducted in the afternoons, between 1 and 5 pm. During these sessions (typically 45–60 min), the animals were anesthetized with Alphaxalone (i.m., 1.85 ml/kg Alfaxan, 10 mg/ml, Jurox, Worcestershire, UK). Peripheral oxygen saturation (SpO₂), heart and respiratory rates were constantly monitored during the image acquisition.

Marmosets reach maturity by 18–24 months of age, produce offspring by 2–3 years and reach old age by 7–8 years of age (Abbott et al. 2003; Missler et al. 1992, 1993a, b; Tardif et al. 2003). The brains of 30 monkeys were scanned, among which 13 (8 males and 5 females) were selected on the basis of having the best image qualities (Table 1). The brain template was designed from 12 healthy young adult

Table 1 List of marmosets used for IMPEC marmoset brain template

Marmoset identity	Age	Sex	Weight (g)	Acquisition (coil)
3287676	4 years 21 days	Male	325	Wrist coil
3287662	4 years 5 months 29 days	Male	357	Wrist coil
3287663	4 years 2 months 26 days	Male	316	Wrist coil
3287665	4 years 7 months 14 days	Female	379	Wrist coil
3287697	4 years 27 days	Male	278	Wrist coil
3287723	4 years 27 days	Male	336	Wrist coil
3287746	3 years 11 months 28 days	Female	280	Wrist coil
3592043	4 years 1 month 9 days	Female	349	Wrist coil
3592124	3 years 10 months 17 days	Female	398	Wrist coil
3592143	3 years 5 months 7 days	Male	368	Wrist coil
3592189	3 years 10 months 6 days	Female	352	Wrist coil
3696327	3 years 9 months 11 days	Male	343	Wrist coil
1853	6 years 14 days	Male	364	Knee coil (acq1k)
1853	6 years 1 month 25 days	Male	364	Wrist coil (acq1w)
1853	8 years 3 months 17 days	Male	347	Wrist coil (acq2w)

monkeys (340 ± 36 g, 3.4–4.6 years old). One of these twelve animals (3287676, 4 years old male) was used for both manual and automatic segmentations. To evaluate our pipeline stability as a function of the acquisition protocol on the same subject, the thirteenth marmoset (monkey 1853) was imaged in the same scanner with a wrist coil and a knee coil at the age of 6 years (acq1w and acq1k), 1 month apart. The same animal was then imaged at the age of 8 years (acq2w) with the wrist coil (Tables 1, 2).

MRI acquisition

Magnetic resonance imaging (MRI) experiments were performed using a 3-T clinical scanner (Achieva; Philips, Best, The Netherlands) located in the Purpan Hospital, Toulouse, France (INSERM UMR 1214). The monkeys were placed in a supine position. High-resolution anatomical images were acquired using a 3-D T_1 -weighted sequence with an antero-posterior (AP) encoding direction. The sagittal plane was chosen to avoid foldover effects.

The brain template was constructed from images obtained with an 8-channel receiving human wrist coil (6.5 cm internal diameter). The knee coil we used for acq1k in animal 1853 was an 8-channel receiving human knee coil with 14 cm internal diameter.

Template construction

In this section, we explain how the IMPEC marmoset brain template was constructed. The template contains an averaged T_1 -weighted (T_1 -W) MR image of marmoset brain, as well as manually segmented brain structures and estimated cortical areas. This information can be automatically mapped to other marmoset brains (see “[Automatic segmentation of marmoset brain images](#)”) to non-invasively estimate the location of cortical areas. More specifically, the template:

1. Provides an efficient tool to rapidly segment marmoset brain structures. Segmentations can also be made more accurate by post-processing, for example using them

Table 2 Summary of the different acquisition conditions with a 3 T scanner

	Wrist coil (monkey 1853_acq2w)	Wrist coil (template + monkey 1853_acq1w)	Knee coil (monkey 1853_acq1k)
Reconstructed voxel (mm)	$0.3 \times 0.3 \times 0.3$	$0.35 \times 0.35 \times 0.35$	$0.4 \times 0.4 \times 0.4$
Field of view (mm)	FH: 105, AP: 74.8, RL: 33.9	FH: 100, AP: 70.8, RL: 39.9	FH: 155, AP: 108.7, RL: 40
Number of slices	113	114	100
TR/TE (ms)	13/5.4	11/4.7 or 12/5.3	12/5.2
Flip angle	8	8	8
Number of signal averages	8	7 or 6	9
Scan duration (min)	48	42 or 36	48

FH foot–head, AP antero–posterior, RL right–left axis, TR repetition time, TE echo time

- as inputs in Bayesian segmentation frameworks such as those implemented in SPM (Ashburner and Friston 2005), where no priors are available for marmosets; and
2. Enables an estimation of cortical area location in marmoset brain images, typically to analyze functional or anatomical–functional data obtained from fMRI or molecular imaging.

The original Paxinos et al. atlas gives coordinates of cortical areas in terms of the classical stereotaxic space coordinates (that is, the horizontal plane is defined as linking the interaural and infraorbital lines), and the same system has been adopted by Woodward et al. (2018). In contrast, many other recent MRI-based 3D templates use the anterior commissure–posterior commissure (AC–PC) line to define the horizontal plane (e.g., (Calabrese et al. 2015)). From our experience in marmoset brain MR imaging, we observed that AC–PC plane and interaural plane are parallel. We chose intra-cerebral planes to set the stereotaxic space of the IMPEC template: the plane through the midline of the left and right hemispheres as the sagittal plane, the AC–PC plane as the horizontal plane, and the plane orthogonal to the horizontal plane passing through the center of the anterior commissure as the coronal plane. The marmoset AC center could be more easily visualized at 3 T than the PC, and for this reason we adopted the AC as the zero point of the antero-posterior axis of the IMPEC template. The position of any point, when navigating in the cortex with 3DSlicer, is given as a distance in millimeters from this origin in the three directions (antero-posterior, right-left, infero-superior).

Figure 1 summarizes the inputs and outputs of our template definition pipeline, details of which are given below.

Average marmoset brain

The variability in the spatial configuration of adult marmoset brains, including the number, location and depth of sulci across subjects, is far less than that observed in adult humans, or even macaque monkeys. As a result, probabilistic template definitions, which are standard for humans (Evans et al. 2012), are not necessarily pertinent. This led us to adopt a simplified template definition strategy where a manual segmentation was carefully performed on a single typical brain and then projected to an average brain shape using the diffeomorphic strategy (Fiot et al. 2014; Vialard et al. 2012b).

The segmented marmoset brain A_{init} was chosen among all the T_1 -W MR images for being close to average in terms of size, and for having one of the best image qualities (case 3287676). The age of this male marmoset was 4 years at the time of acquisition, and the image had a resolution of $0.35 \times 0.35 \times 0.35$ mm per voxel (details are given in “Subjects”). To make A_{init} mathematically averaged, it was deformed towards the Karcher mean (Karcher 1977) of 11 other brain images acquired on marmosets having a similar age (around 4 years, between 3.4 and 4.6 years; Table 1). The main advantages of this method are that it fully preserves the topology of the brain structures, and that it only induces a minor smoothing of the transported shape compared with the original one, due to image resampling using only one displacement field.

In practice, this iterative method was performed as follows: we denoted A_{cur} as the average image at the current iteration and I_n , n in $[1, \dots, 11]$, the 11 other brain images. We initiated A_{cur} as equal to the empirically selected average brain A_{init} . Diffeomorphic registration of A_{cur} on the different images I_n was then performed using the method of (Vialard et al. 2012a), with a Gaussian kernel of 3 mm, which

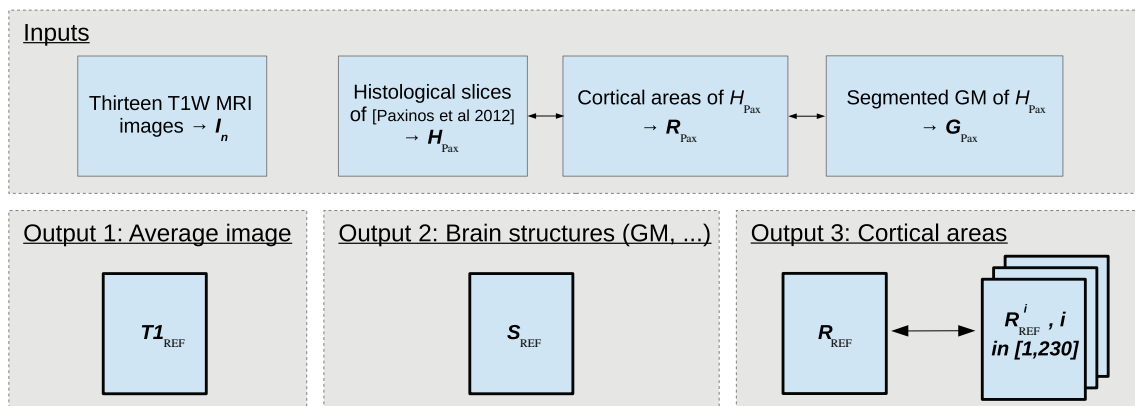


Fig. 1 Inputs and outputs of the template definition pipeline. The reference image $T1_{\text{REF}}$ is the diffeomorphic average of eleven T_1 -W MRI marmoset brain images. The segmentation of its different structures

(gray matter, white matter, ...) is S_{REF} and its estimated cortical areas are in R_{REF} . Image R_{REF}^i contains the blurred segmentation of each cortical area i

resulted in 11 initial momenta M_n . For a given kernel and a moving image (here A_{cur}), an initial momentum was a scalar field that fully encoded the invertible displacement field that matched the moving image and the fixed image (here I_n). Initial momenta have interesting mathematical properties: in particular, the average deformation to project A_{cur} towards the average shape of the I_n is the one encoded by the mean initial momentum $M_{\text{cur}} = \text{mean}(M_1, \dots, M_{11})$. We then projected A_{cur} using the average displacement field M_{cur} , and considered this transformed image as A_{cur} at the next iteration. Resampling an image has the property to smooth its boundaries. In order to avoid over-smoothing A_{cur} iteration after iteration, we use the following strategy: The image A_{cur} is actually modeled as the deformation of A_{init} through a diffeomorphism Φ_{cur} (i.e. $A_{\text{cur}} = A_{\text{init}} \circ (\Phi_{\text{cur}})^{-1}$). At each iteration, we denote φ_{upd} the deformation of A_{cur} with M_{cur} . The whole deformation Φ_{cur} is then updated by being composed with φ_{upd} (i.e. $\Phi_{\text{cur}} = \Phi_{\text{cur}} \circ \varphi_{\text{upd}}$). The image A_{cur} is finally updated using a single resampling using the relation $A_{\text{cur}} = A_{\text{init}} \circ (\Phi_{\text{cur}})^{-1}$. As shown in (Vialard et al. 2012b), when the shapes are sufficiently regular, this process converges after a few iterations; this was the case here, given the fact that marmoset brains are lissencephalic. When computing the average shape, negligible deformations were observed after five iterations only, and a maximal deformation of 1.07 mm was obtained. We denote ϕ_{Kar} the whole deformation, which corresponds to Φ_{cur} at the end of the algorithm, and $T1_{\text{REF}} = A_{\text{init}} \circ (\phi_{\text{Kar}})^{-1}$ the reference marmoset brain image obtained at the algorithm convergence.

Brain structures

In the proposed template, reference brain structures were manually segmented in the marmoset brain image A_{init} . Fine manual segmentation was performed using the Gimp 2.8.10 software (<https://www.gimp.org/>) after a first coarse segmentation performed using the active contour segmentation algorithm (Yushkevich et al. 2006; Zhu and Yuille 1996) of ITK-Snap (<http://www.itksnap.org/>). Manual segmentation of the gray matter (GM), white matter (WM) and intracerebral (ventricles) plus subarachnoid space (CSF) of A_{init} was performed slice by slice on coronal planes on $T1$ -W MR images from the 4-year-old marmoset (case 3287676). The quality of the segmentation was also carefully checked on both axial and sagittal planes with MRICron software.

In addition to these classic cerebral compartments, we also segmented the brain stem, the cerebellum and the olfactory bulb. We finally partially segmented the hippocampus focusing our attention on the middle and anterior parts of the hippocampus where this structure can be accurately delineated given that it is boarded ventrally and laterally by white matter, and dorsally by the lateral ventricle. On the rostral part, this region is limited by a coronal plane situated just

behind the pituitary stalk. The caudal part of this region is limited by a plane passing through the interpeduncular fossa.

Subcortical structures which can be identified, but not clearly delineated in the images obtained with a 3 T scanner, were not included in the manual segmentation step.

Volume reconstruction of the segmented slices was performed using the Convert3D tool distributed with ITK-Snap. Projection of the segmentation onto $T1_{\text{REF}}$ was finally performed using the deformation ϕ_{Kar} with nearest neighbor interpolation. In what follows, S_{REF} refers to the segmentation of $T1_{\text{REF}}$.

Cortical areas

In addition to S_{REF} , we estimated the different cortical area locations of $T1_{\text{REF}}$. The goal of these area locations is to make it simple to quantify how likely different voxels of other marmoset brains are to belong to specific cortical areas, based on atlas propagation. We denote R_{REF}^i the location of cortical area i in $T1_{\text{REF}}$, i in $[1, 230]$. For instance, $R_{\text{REF}}^1(x)$ equals 1 means that point x of $T1_{\text{REF}}$ is in the first cortical area of Online Appendix 1 (i.e., in the cortical area A10), and $R_{\text{REF}}^1(x)$ equals 0 means that x is outside this area. This information is also summarized in the mask R_{REF} that contains the most likely indices i of all points x of $T1_{\text{REF}}$.

To build the R_{REF}^i , our initial material was the information defined on the left hemisphere of a 3.2-year-old female marmoset proposed by Paxinos et al. (2012). We used the freely distributed pdf version, available from <http://www.marmosetbrain.org/reference>, with agreement from the authors. The cortical areas in this individual were thoroughly segmented using histological slices having a resolution of 0.04×0.04 mm and sampled on the frontal axis every 0.5 mm. These histological slices were recomposed as a 3D image H_{Pax} using the *3D Brain Atlas Reconstructor software* (Majka et al. 2012) and made available online via the *3D Brain Atlas Reconstructor website* [(Majka et al. 2013), <http://3dbars.org>] as well as the *Scalable Brain Atlas (SBA) website* [(Bakker et al. 2015), <https://scalablebrainatlas.incf.org/>]. Segmentation of the gray matter in this 3D volume, which we denote G_{Pax} , is distributed on the SBA website. One hundred and fifteen cortical areas (R_{Pax}) are also distinguished at the gray matter outer surface of this image.

We first symmetrized the segmented gray matter G_{Pax} to mimic a gray level segmentation in the two hemispheres. The resulting segmentation in the two hemispheres was then mapped to the manually segmented gray matter of A_{init} : manual rigid alignment was performed before the non-rigid registration of the segmented images using the LogDemons registration algorithm (Vercauteren et al. 2008) implemented in uTIlzreg (<https://sourceforge.net/projects/utilzreg/>). Twelve manually selected landmarks, mainly corresponding to locations within sulci, were used to accurately

register the sulci where the contrast was not sufficient in the segmented images. These steps were performed in the image domain of A_{init} and resulted in a deformation ϕ_{Pax} which was used hereafter to transport the cortical areas of Paxinos et al. (2012) into the image domain of A_{init} .

We now explain how the cortical areas R_{Pax} were transported into the reference image domain. We first propagated the cortical areas labels R_{Pax} from the outer surface of the gray matter to its volume, i.e., to all voxels of G_{Pax} labeled as within the gray matter. Each of these voxels received the nearest known cortical area label at the cortex surface, using Euclidian distances. The resulting label map was then symmetrized with the same properties as those used for G_{Pax} , as described in the previous paragraph. The original cortical areas have the same label as in R_{Pax} and the symmetrized areas have the label of R_{Pax} plus 115 (from 116 to 230). This symmetric labels map was finally transported to the reference image domain of $T1_{\text{REF}}$ using the deformation $(\phi_{\text{Kar}})^{-1} \circ (\phi_{\text{Pax}})^{-1}$, i.e., the deformation used to project the labels to A_{init} and then $T1_{\text{REF}}$, with nearest neighbor interpolation. We denote R_{REF} the resulting label map of reference cortical areas.

We emphasize that the R_{REF}^i do not represent the cortical areas of $T1_{\text{REF}}$ but rather their estimates. The registration ϕ_{Pax} was computed using images representing the segmented cortex, although the spatial distribution of the cortical areas is likely to be variable from one marmoset to another (Majka et al. 2016). An ongoing study reveals that variability exists but that areas tend to maintain their spatial relationship to each other, and to gross anatomical landmarks such as sulci and main folds as the dorsal midline (P. Majka and M. G. P. Rosa, unpublished observations). Besides, delineations of another marmoset's cortex reached similar conclusions regarding the location and proportional size of the areas (Hashikawa et al. 2015). Moreover, the original cortical areas were symmetrized; although they may not be purely symmetric, experience from histological parcellation of a larger sample of individuals (available from marmosetbrain.org) suggests that this factor may be negligible (MGP Rosa, unpublished observations). To account for spatial uncertainty in the R_{REF}^i , the cortical areas were then independently smoothed using Gaussian kernel convolution with a standard deviation of 1 mm. This level of smoothing was empirically determined based on providing a good tradeoff between too much- and not enough blurring of the original segmented cortical areas. This resulted in the different R_{REF}^i , i in $[1, 230]$.

Note that, to provide a more global view of the different cortical regions in our template, we additionally propose groupings of areas into larger ensembles, such as occipital, temporal, parietal, limbic, insular, and frontal, the last one being composed of prefrontal and motor sub-regions (see

Online Appendix 1, colors have been arbitrarily chosen for the cortical regions).

Finally, the information contained in the R_{REF}^i was summarized in the mask R_{REF} that contains the most likely indices i of all points x of $T1_{\text{REF}}$. To do so, we simply build R_{REF} using the following formula: $R_{\text{REF}}(x) = \text{argmax}_i R_{\text{REF}}^i(x)$.

Automatic segmentation of marmoset brain images

Overview

In addition to the segmented brain structures and cortical areas/regions, we provide a segmentation pipeline that automatically projects the information S_{REF} , R_{REF} and R_{REF}^i from the reference image domain $T1_{\text{REF}}$ to any given tested $T1$ -W MR image I_{TST} of the marmoset brain. The segmentation pipeline was based on an atlas propagation strategy that fully exploits the segmented template described in “[Template construction](#)”. The transported brain structures S_{TST} are a coarse segmentation of I_{TST} , which can be used directly for most applications. They can also be conveniently used as priors in a Bayesian segmentation strategy such as the one of SPM (Ashburner and Friston 2005). As mentioned in “[Results](#)”, the transported cortical areas/regions map R_{TST} can be directly considered as the segmentation of I_{TST} cortical areas/regions. To additionally reflect the spatial uncertainty of the structure boundaries, the user can also use the blurred maps of R_{TST}^i .

Our segmentation pipeline was coded in Python with as few dependencies as possible, all of them being freely available online. Specifically, the dependencies were (1) the *Numpy* library, which is ubiquitously used for numerical mathematics under Python, and (2) the SimpleITK library (<http://www.simpleitk.org/>), which can load and save most image formats used in neuroimaging under Python and which proposes pre-compiled parallel algorithms in C++ for biomedical image registration and segmentation among others.

Our pipeline can be run in a command-line environment using, e.g., the freely available Python distribution Anaconda (<https://www.continuum.io/downloads>). The results shown were obtained using the default Python distribution of Linux Ubuntu 16.04. The command-line pipeline also successfully worked using Anaconda under Windows and Mac OS X. When using the command-line environment, we recommend ITK-Snap (<http://www.itksnap.org/>) for image visualization. User instructions are given in Online Appendix 2.

To make our script more user-friendly, we also fully integrated it as a Slicer module (<https://www.slicer.org/>) (Fedorov et al. 2012). The slicer interface is illustrated on Fig. 2. Slicer is an open-source software for medical image

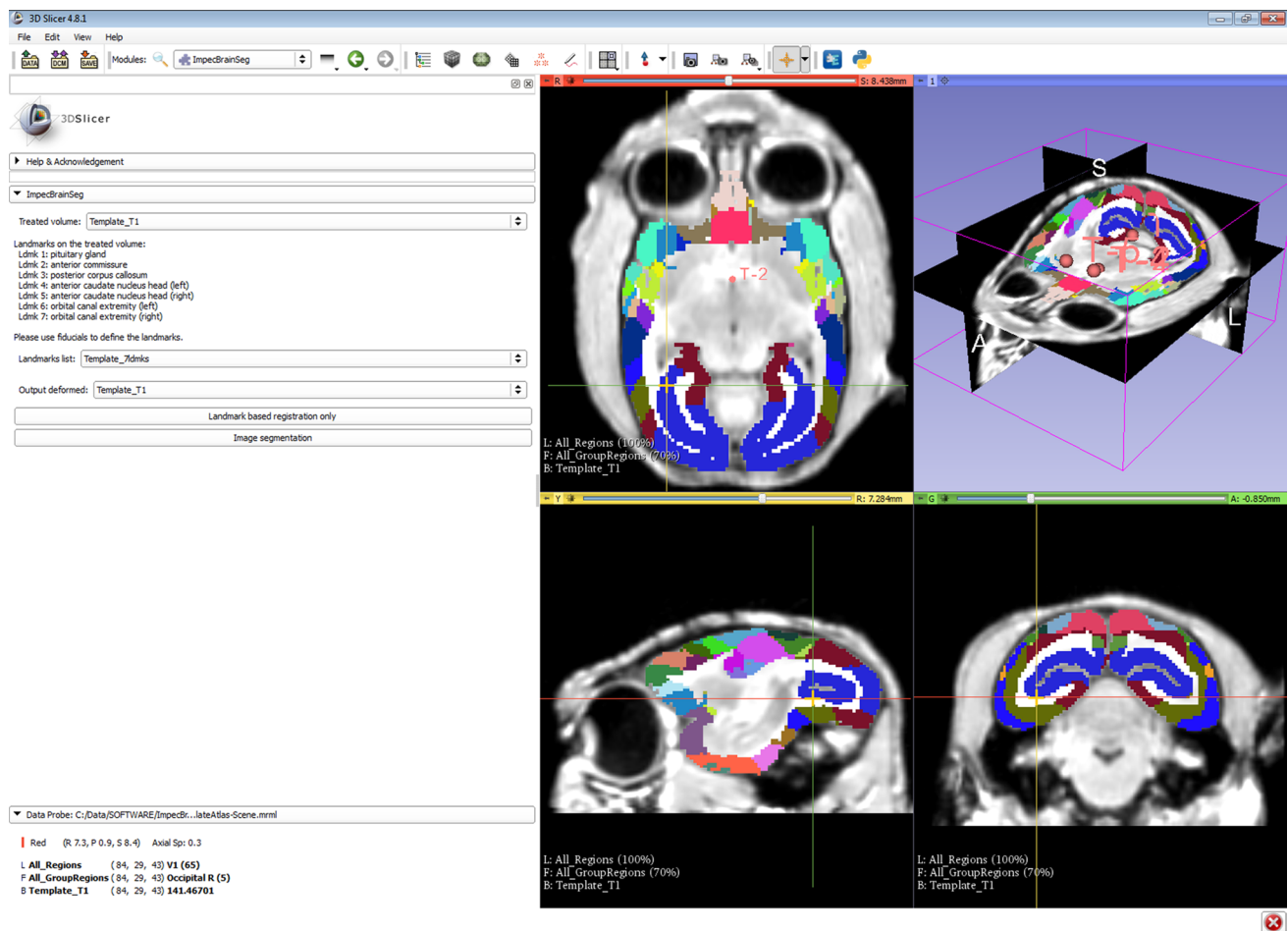


Fig. 2 Overview of the Slicer interface. The ImpecBrainSeg widget that allows to parameterize and to launch the computations is on the left. Image and results visualization in 2D or 3D is made on the right

processing and three-dimensional visualization. An interesting aspect of Slicer is that it can be extended with Python modules giving access to many of its functionalities without recompiling the whole software and its dependencies. It was then relatively straightforward to incorporate the command-line pipeline into Slicer. For the end user, using Slicer has also the advantage that landmarks definition, image segmentation and results visualization can be made in the same environment without executing any command line. Installation is also simple as Python and SimpleITK are integrated to Slicer binaries for Windows, Mac and Linux. As for the command-line interface, user instructions for Slicer are given in Online Appendix 2.

Technical details

Coarse rigid registration of $T1_{REF}$ to I_{TST} is first performed as follows: the script automatically aligns manually defined landmarks of I_{TST} on those of $T1_{REF}$. Landmarks definition is developed in “[Landmarks selection](#)”.

The filter *LandmarkBasedTransformInitializerFilter* of *SimpleITK* is used for this purpose. Accurate rigid registration is then performed using the *ImageRegistrationMethod* of *SimpleITK* with *ANTSNeighborhoodCorrelation* as a similarity metric. Non-rigid registration is finally performed using the registration algorithm of *ImageRegistrationMethod* for displacement field again with *ANTSNeighborhoodCorrelation* as a similarity metric (Avants et al. 2011). Deformation regularization is relatively close to what would be done in a Demons registration algorithm (Thirion 1998) with a fluid and a diffusion regularization of 9 mm and 1 mm, respectively. The segmentation pipeline is summarized in Fig. 3.

Note that we recommend performing bias field correction on I_{TST} before registering the reference information to its domain. To achieve this, the *N4BiasFieldCorrection* strategy of *SimpleITK* (Tustison et al. 2010), which is also available as a Slicer module, can be used.

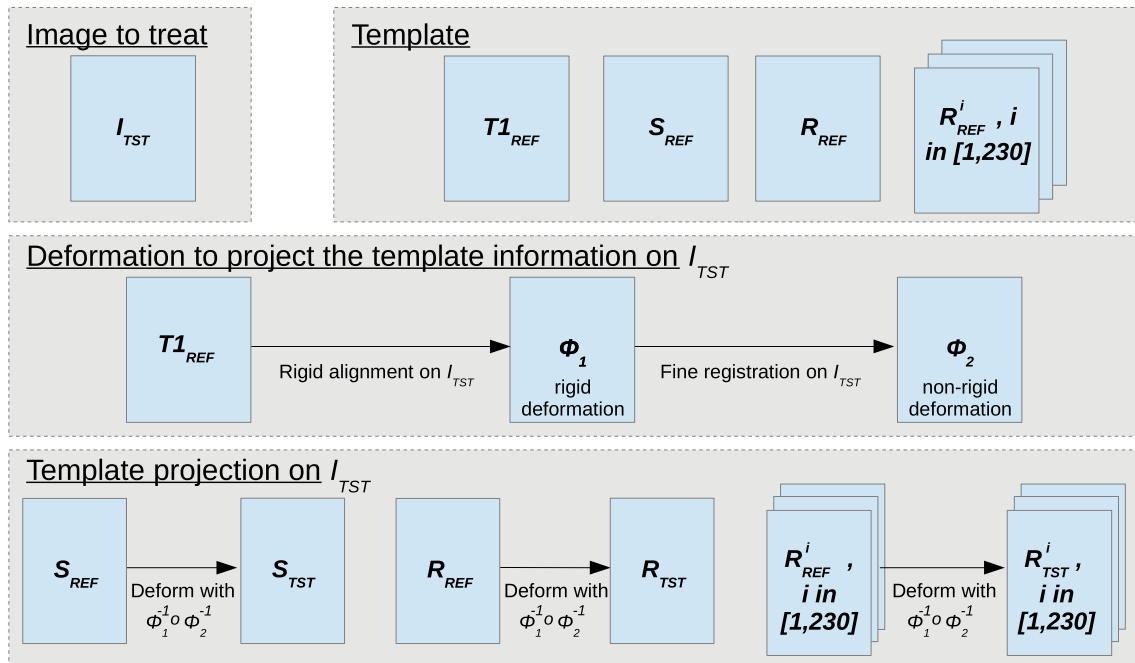


Fig. 3 Pipeline used to project the template information on a test image I_{TST} . The reference image $T1_{REF}$ is first aligned and registered on I_{TST} . The estimated information is then used to project the structures' segmentation S_{REF} and the estimated cortical areas R_{REF} and R_{REF}^i , i in $[1, 230]$

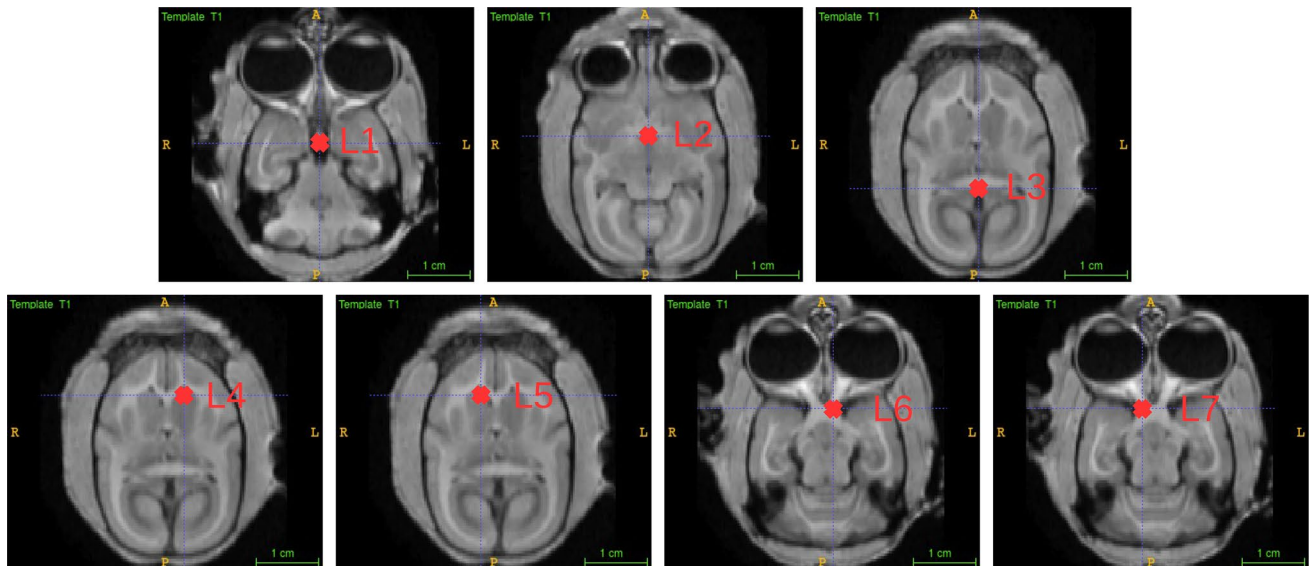


Fig. 4 Location of the 7 reference landmarks on the T_1 template image $T1_{REF}$. Corresponding points have to be picked on I_{TST} before segmentation

Landmarks selection

The user has to pick seven landmarks in the segmented image to make possible a coarse template alignment before a more accurate registration (Fig. 4). The landmarks, chosen to be distributed along the antero/posterior and the

dorso-ventral axes of the brain, are the followings: (L1: pituitary gland), (L2: anterior commissure), (L3: posterior corpus callosum), [L4: anterior caudate nucleus head (left)], [L5: anterior caudate nucleus head (right)], [L6: orbital canal extremity (left)], and [L7: orbital canal extremity (right)].

Results

Quantitative assessment of manual vs. automated segmentation

To quantify the stability of our segmentation pipeline, three T_1 -W MR images were acquired on a 6-year-old animal (case 1853) under different conditions. The brain was imaged, 1 month apart, with two different coils (human knee- and wrist coils). A third acquisition was performed 2 years later with the wrist coil, under the same conditions. All images obtained with these procedures were distinct from those used to create the template.

An expert delineated manual segmentations of the cortex on the images. For each image, three consecutive slices were segmented in the coronal plane. In parallel, segmentations of the cortex were obtained automatically with the registration-based approach proposed here, after undergoing prior bias field correction. An example of a manually segmented slice and its corresponding automatic segmentation (before and after binarization) is given in Fig. 5. Robustness of our segmentation approach was assessed quantitatively with Dice coefficients, a measure of the similarity between automatic segmentations and their ground truth, i.e., manual segmentations, which was computed as described in (Taha and Hanbury 2015). Since the output segmentations are smooth, i.e., with values between 0 and 1, they were binarized with automatically computed threshold prior to their comparison with binary manual segmentations. Dice coefficients range between 0 (no segmentation overlap) and 1 (perfect segmentation overlap). Results are summarized in Table 3 and show good overlaps.

Qualitative assessment of cortical atlas mapping

Two T_1 -W MRI acquisitions were performed on the same animal at the same age (1 month delay between the 2 acquisitions), with the same scanner and the same sequence (parameters given in “Methods”). The only key difference is the coil used with the scanner device (knee and wrist coils). We have compared the propagation of the

Table 3 Dice coefficients computed from manual vs. binarized automated segmentations of the cortex obtained from T_1 -W MR images of the same marmoset acquired in 3 different acquisition conditions (coil and age)

Slice	Knee coil 6 years old	Wrist coil 6 years old	Wrist coil 8 years old
1	0.8063	0.88636	0.8979
2	0.88363	0.92	0.9033
3	0.90289	0.91208	0.8912

Rows correspond to values obtained for three adjacent coronal slices

cortical atlas to the T_1 -W image in both conditions, which apart from precision differences did not depict major differences, especially in the largest areas, since we are considering the same animal at about the same age. Similar results were obtained when using the wrist coil instead of the knee one. In addition, a third acquisition was obtained with the same scanner, wrist coil and sequence parameters (Table 2) 2 years later. The results are shown in Fig. 6 for the acquisition performed on the then 8-year-old marmoset with the wrist coil. In Fig. 6a, we show the estimated cortical atlas in the axial, sagittal and coronal planes, plus a 3D volume rendering. A corresponding atlas of larger cortical regions is shown in Fig. 6b. It consists of 14 different regions for the two hemispheres, each composed of many cortical areas (see Online Appendix 1).

We emphasize that these are only estimated cortical areas/regions. Indeed, to visualize an atlas such as the one shown here, only the label of the region with the highest score was kept for each voxel. More precisely, a K-nearest neighbor based thresholding algorithm was performed to preserve local homogeneity in regions.

If we look closer at a particular voxel’s coordinates in the brain cortex, we will find that the score of actually being in the area corresponding to the attributed label, or color in the figure, is lower than 1. This is the case particularly near the boundary between adjacent areas, where estimates might overlap, resulting in two or more complementary scores. As an example, actual results were investigated at two different coordinates. The first one was



Fig. 5 Overlay between a coronal slice and the corresponding segmentation of the cortex for the T_1 -W MR image acquired on an 8-year-old marmoset using the wrist coil. **a** Smooth automatic segmentation, **b** automatic segmentation and **c** manual segmentation (ground truth)

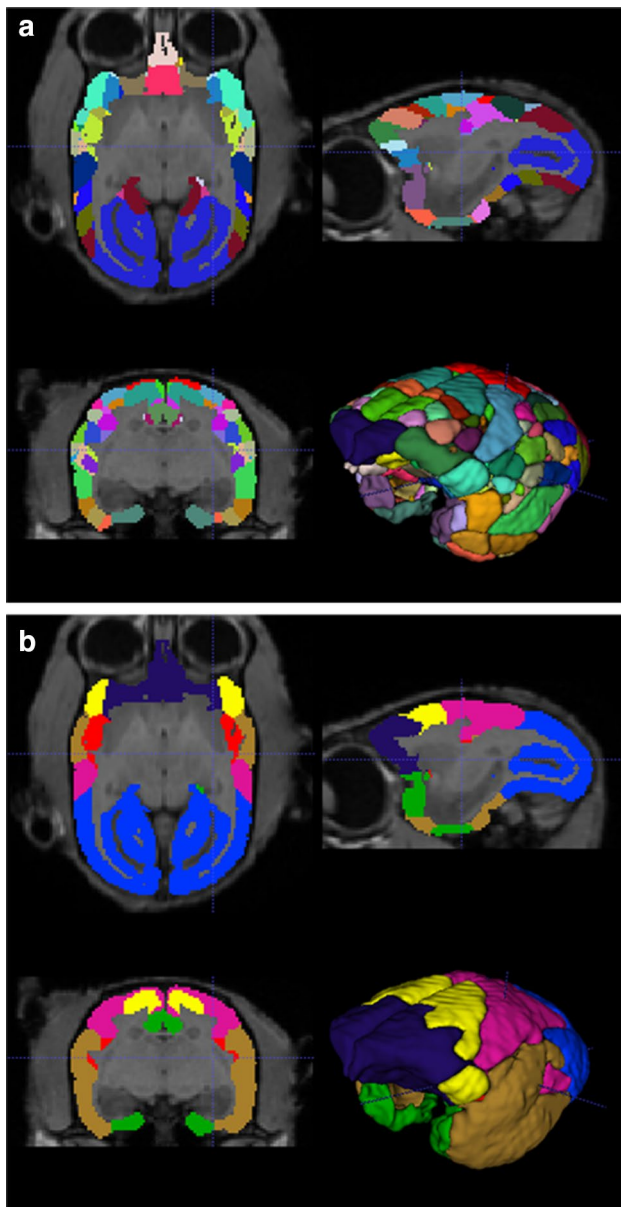


Fig. 6 Atlas mapping with T_1 -W MRI of an 8-year-old marmoset monkey acquired on a 3 T MRI scanner with a wrist receiving coil. **a** Represents the Paxinos atlas of cortical areas (Paxinos et al. 2012) mapped to the original image, whereas **b** represents the mapping of larger cortical regions (see Online Appendix 1 for regions–areas correspondences). Colors for the cortical areas have been chosen similar to those shown in Paxinos et al. (2012). In each case, axial, sagittal and coronal 2D views are given in the top left, top right, bottom left panels, respectively, and a corresponding 3D view of the estimated cortical areas/regions is shown in the bottom right panel

picked in the middle of V1, a large visual area, where the confidence is in principle higher, whereas the second point was chosen to be attributed to the parietal region where areas are smaller and the overlap between their location maps is consequently higher (see Online Appendix 3).

Discussion

Here, we describe the creation of a new 3D marmoset brain template (IMPEC template) that distinguishes three brain compartments (gray matter, white matter and CSF), four structures (brain stem, cerebellum, olfactory bulb, visible points of the hippocampus) and 230 cortical areas, 115 in each hemisphere. The cortical areas are also gathered into 7 brain regions in each hemisphere (occipital, temporal, parietal, limbic, insular, frontal-prefrontal and frontal-motor regions). Our template is diffeomorphic in the sense that it was thoroughly defined on a single marmoset brain image and then transported onto an average marmoset brain shape, using a diffeomorphic strategy that fully preserves the brain topology. Unlike other available templates that use the definition of cortical areas proposed by Paxinos and collaborators (Hashikawa et al. 2015; Majka et al. 2016), the IMPEC template is based on an average of multiple (12) individuals.

We additionally described a marmoset brain segmentation pipeline that takes advantage of this template. This pipeline is coded in Python with extensive use of SimpleITK routines so that it can be run on Windows, Mac or Linux. It can be either executed using a command-line interface or as a module of the Slicer software. Although these versions make use of the same SimpleITK algorithms with the same parameters, they target different types of users: the command-line interface version can be scripted and is made for users familiar with unix-like environment, while the Slicer version does not require to execute any command line and can then be seen as more accessible to many users.

Results show that our segmentation pipeline performs well on different marmoset brain images acquired using different coils in a 3 T scanner. The segmented brain structures and estimated cortical areas/regions can then be reasonably used directly for most applications. For instance, it can be used to non-invasively estimate the extents of cortical lesions, including giving scores of involvement of specific areas, or to define seeds for tractography studies. T_1 - or T_2 -weighted images can also be optionally registered to the template and to its associated segmentations and location maps, for further group analyses. If very accurate segmentations are required, e.g., when estimating the cortical thickness, the segmented brain structures can also be used as priors for more advanced Bayesian segmentation algorithms, such as those of SPM. In the future, we will use it for longitudinal studies of the brain morphometry and for cortical areas estimation in anatomical MR images combined with functional PET images. We acknowledge that the present study focuses on cortex. This limitation has to be addressed by future work, using higher magnet MRI, to provide reliable segmentation of thalamic structures and thus enlarge the template. We finally want to emphasize that our template

definition framework and segmentation pipeline were used for marmoset brains but could also be directly reused for any other lissencephalic species.

Acknowledgements We would like to thank Tristan Chaplin and Piotr Majka for generating the 3D map of cytoarchitectural areas of the marmoset brain derived from the atlas of (Paxinos et al. 2012). Our gratitude goes to MRI platform (INSERM UMR1214) for their priceless assistance. We also thank the staff of the CerCo animal rearing facilities and Emilie Rapha for their help with animal preparation and monitoring.

Funding This work was financially supported by the University Paul Sabatier, Toulouse 3 (AO1 MST2I_2013) and the Toulouse Mind and brain Institute (TMBI, AO2015). A.S. Ph.D. was Granted by University Paul Sabatier/Toulouse 3 and Foundation for Medical Research (FDT20160435166). The participation of MGP Rosa was funded by the Australian Research Council's Centre of Excellence for Integrative Brain function (CE140100007).

Compliance with ethical standards

Conflict of interest The authors declare that they have no conflict of interest.

Research involving animals/ethical approval All applicable international, national and/or institutional guidelines for the care and use of animals were followed. All procedures performed in studies involving animals were in accordance with the ethical standards of the institution or practice at which the studies were conducted. The project received the regional (MP/03/76/11/12) and the governmental authorization from the MENESR (project 05215.03).

References

- Abbott DH, Barnett DK, Colman RJ, Yamamoto ME, Schultz-Darken NJ (2003) Aspects of common marmoset basic biology and life history important for biomedical research. *Comp Med* 53:339–350
- Amlien IK, Fjell AM, Tamnes CK, Grydeland H, Krogsrud SK, Chaplin TA, Rosa MGP, Walhovd KB (2016) Organizing principles of human cortical development—thickness and area from 4 to 30 years: insights from comparative primate neuroanatomy. *Cereb Cortex* 26:257–267
- Ashburner J, Friston KJ (2005) Unified segmentation. *Neuroimage* 26:839–851
- Avants BB, Tustison NJ, Song G, Cook PA, Klein A, Gee JC (2011) A reproducible evaluation of ANTs similarity metric performance in brain image registration. *Neuroimage* 54:2033–2044
- Bakker R, Tiesinga P, Kotter R (2015) The scalable brain atlas: instant web-based access to public brain atlases and related content. *Neuroinformatics* 13:353–366
- Bakola S, Burman KJ, Rosa MGP (2015) The cortical motor system of the marmoset monkey (*Callithrix jacchus*). *Neurosci Res* 93:72–81
- Belcher AM, Yen CC, Notardonato L, Ross TJ, Volkow ND, Yang Y, Stein EA, Silva AC, Tomasi D (2016) Functional connectivity hubs and networks in the awake marmoset brain. *Front Integr Neurosci* 10:9
- Bock NA, Kocharyan A, Liu JV, Silva AC (2009) Visualizing the entire cortical myelination pattern in marmosets with magnetic resonance imaging. *J Neurosci Methods* 185:15–22
- Bourne JA, Rosa MGP (2006) Hierarchical development of the primate visual cortex, as revealed by neurofilament immunoreactivity: early maturation of the middle temporal area (MT). *Cereb Cortex* 16:405–414
- Burkart JM, Finkenwirth C (2015) Marmosets as model species in neuroscience and evolutionary anthropology. *Neurosci Res* 93:8–19
- Burman KJ, Palmer SM, Gamberini M, Rosa MGP (2006) Cytoarchitectonic subdivisions of the dorsolateral frontal cortex of the marmoset monkey (*Callithrix jacchus*), and their projections to dorsal visual areas. *J Comp Neurol* 495:149–172
- Burman KJ, Lui LL, Rosa MGP, Bourne JA (2007) Development of non-phosphorylated neurofilament protein expression in neurons of the New World monkey dorsolateral frontal cortex. *Eur J Neurosci* 25:1767–1779
- Burman KJ, Reser DH, Richardson KE, Gaulke H, Worthy KH, Rosa MGP (2011) Subcortical projections to the frontal pole in the marmoset monkey. *Eur J Neurosci* 34:303–319
- Burman KJ, Bakola S, Richardson KE, Reser DH, Rosa MGP (2014) Patterns of afferent input to the caudal and rostral areas of the dorsal premotor cortex (6DC and 6DR) in the marmoset monkey. *J Comp Neurol* 522:3683–3716
- Burman KJ, Bakola S, Richardson KE, Yu HH, Reser DH, Rosa MGP (2015) Cortical and thalamic projections to cytoarchitectural areas 6Va and 8C of the marmoset monkey: connectionally distinct subdivisions of the lateral premotor cortex. *J Comp Neurol* 523:1222–1247
- Calabrese E, Hickey P, Hulette C, Zhang J, Parente B, Lad SP, Johnson GA (2015) Postmortem diffusion MRI of the human brainstem and thalamus for deep brain stimulator electrode localization. *Hum Brain Mapp* 36:3167–3178
- Converse AK, Aubert Y, Farhoud M, Weichert JP, Rowland IJ, Ingrisano NM, Allers KA, Sommer B, Abbott DH (2012) Positron emission tomography assessment of 8-OH-DPAT-mediated changes in an index of cerebral glucose metabolism in female marmosets. *Neuroimage* 60:447–455
- Evans AC, Janke AL, Collins DL, Baillet S (2012) Brain templates and atlases. *Neuroimage* 62:911–922
- Fedorov A, Beichel R, Kalpathy-Cramer J et al (2012) 3D Slicer as an image computing platform for the quantitative imaging network. *Magn Reson Imaging* 30:1323–1341
- Fiot JB, Raguet H, Risser L, Cohen LD, Fripp J, Vialard FX, Alzheimer's Disease Neuroimaging I (2014) Longitudinal deformation models, spatial regularizations and learning strategies to quantify Alzheimer's disease progression. *Neuroimage Clin* 4:718–729
- Fuster JM (2001) The prefrontal cortex—an update: time is of the essence. *Neuron* 30:319–333
- Fuster JM (2002) Frontal lobe and cognitive development. *J Neurocytol* 31:373–385
- Garea-Rodriguez E, Schlumbohm C, Czeh B, König J, Helms G, Heckmann C, Meller B, Meller J, Fuchs E (2012) Visualizing dopamine transporter integrity with iodine-123-FP-CIT SPECT in combination with high resolution MRI in the brain of the common marmoset monkey. *J Neurosci Methods* 210:195–201
- Gebhard R, Zilles K, Schleicher A, Everitt BJ, Robbins TW, Divac I (1995) Parcellation of the frontal cortex of the New World monkey *Callithrix jacchus* by eight neurotransmitter-binding sites. *Anat Embryol (Berl)* 191:509–517
- Ghahremani M, Hutchison RM, Menon RS, Everling S (2016) Frontoparietal functional connectivity in the common marmoset. *Cereb Cortex*. <https://doi.org/10.1093/cercor/bhw198>
- Hashikawa T, Nakatomi R, Iriki A (2015) Current models of the marmoset brain. *Neurosci Res* 93:116–127
- Karcher H (1977) Riemannian center of mass and mollifier smoothing. *Commun Pure Appl Math* 30:509–541

- Krubitzer LA, Kaas JH (1990) The organization and connections of somatosensory cortex in marmosets. *J Neurosci* 10:952–974
- Lui LL, Bourne JA, Rosa MGP (2006) Functional response properties of neurons in the dorsomedial visual area of New World monkeys (*Callithrix jacchus*). *Cereb Cortex* 16:162–177
- Majka P, Kublik E, Furga G, Wojcik DK (2012) Common atlas format and 3D brain atlas reconstructor: infrastructure for constructing 3D brain atlases. *Neuroinformatics* 10:181–197
- Majka P, Kowalski JM, Chlodzinska N, Wojcik DK (2013) 3D brain atlas reconstructor service—online repository of three-dimensional models of brain structures. *Neuroinformatics* 11:507–518
- Majka P, Chaplin TA, Yu HH, Tolpygo A, Mitra PP, Wojcik DK, Rosa MGP (2016) Towards a comprehensive atlas of cortical connections in a primate brain: mapping tracer injection studies of the common marmoset into a reference digital template. *J Comp Neurol* 524:2161–2181
- Mansouri FA, Koechlin E, Rosa MGP, Buckley MJ (2017) Managing competing goals—a key role for the frontopolar cortex. *Nat Rev Neurosci* 18:645–657. <https://doi.org/10.1038/nrn.2017.111>
- Marmoset Genome Sequencing and Analysis Consortium (2014) The common marmoset genome provides insight into primate biology and evolution. *Nat Genet* 46:850–857
- Marx V (2016) Neurobiology: learning from marmosets. *Nat Methods* 13:911–916
- Meyer JS, Brevard ME, Piper BJ, Ali SF, Ferris CF (2006) Neural effects of MDMA as determined by functional magnetic resonance imaging and magnetic resonance spectroscopy in awake marmoset monkeys. *Ann N Y Acad Sci* 1074:365–376
- Miller CT, Freiwald WA, Leopold DA, Mitchell JF, Silva AC, Wang X (2016) Marmosets: a neuroscientific model of human social behavior. *Neuron* 90:219–233
- Missler M, Wolff JR, Heger W, Merker HJ, Treiber AM, Scheib R, Crook GA (1992) Developmental biology of the common marmoset: proposal for a “postnatal staging”. *J Med Primatol* 21:285–298
- Missler M, Eins S, Merker HJ, Rothe H, Wolff JR (1993a) Pre- and postnatal development of the primary visual cortex of the common marmoset. I. A changing space for synaptogenesis. *J Comp Neurol* 333:41–52
- Missler M, Wolff A, Merker HJ, Wolff JR (1993b) Pre- and postnatal development of the primary visual cortex of the common marmoset. II. Formation, remodelling, and elimination of synapses as overlapping processes. *J Comp Neurol* 333:53–67
- Mitchell JF, Leopold DA (2015) The marmoset monkey as a model for visual neuroscience. *Neurosci Res* 93:20–46
- Newman JD, Kenkel WM, Aronoff EC, Bock NA, Zametkin MR, Silva AC (2009) A combined histological and MRI brain atlas of the common marmoset monkey, *Callithrix jacchus*. *Brain Res Rev* 62:1–18
- Nummela SU, Jovanovic V, de la Mothe L, Miller CT (2017) Social context-dependent activity in marmoset frontal cortex populations during natural conversations. *J Neurosci* 37:7036–7047
- Okano H, Mitra P (2015) Brain-mapping projects using the common marmoset. *Neurosci Res* 93:3–7
- Okano H, Sasaki E, Yamamori T, Iriki A, Shimogori T, Yamaguchi Y, Kasai K, Miyawaki A (2016) Brain/MINDS: a Japanese National Brain Project for Marmoset Neuroscience. *Neuron* 92:582–590
- Palazzi X, Bordier N (2008) The marmoset brain in stereotaxic coordinates. Springer, Berlin
- Paxinos G, Watson C, Petrides M, Rosa MGP, Tokuno H (2012) The marmoset brain in stereotaxic coordinates. Elsevier Academic Press, Cambridge
- Preuss TM, Goldman-Rakic PS (1991) Myelo- and cytoarchitecture of the granular frontal cortex and surrounding regions in the strepsirrhine primate Galago and the anthropoid primate Macaca. *J Comp Neurol* 310:429–474
- Prins NW, Pohlmeier EA, Debnath S, Mylavarapu R, Geng S, Sanchez JC, Rothen D, Prasad A (2017) Common marmoset (*Callithrix jacchus*) as a primate model for behavioral neuroscience studies. *J Neurosci Methods* 284:35–46
- Sadoun A, Strelnikov K, Bonte E, Fonta C, Girard P (2015) Cognitive impairment in a young marmoset reveals lateral ventriculomegaly and a mild hippocampal atrophy: a case report. *Sci Rep* 5:16046
- Sasaki E (2015) Prospects for genetically modified non-human primate models, including the common marmoset. *Neurosci Res* 93:110–115
- Sawiak SJ, Shiba Y, Oikonomidis L, Windle CP, Santangelo AM, Grydeland H, Cockcroft G, Bullmore ET, Roberts AC (2018) Trajectories and milestones of cortical and subcortical development of the marmoset brain from infancy to adulthood. *Cereb Cortex* 28:4440–4453
- Senoo A, Tokuno H, Watson C (2015) Mini-atlas of the marmoset brain. *Neurosci Res* 93:128–135
- Silva AC (2017) Anatomical and functional neuroimaging in awake, behaving marmosets. *Dev Neurobiol* 77:373–389
- Solomon SG, Rosa MGP (2014) A simpler primate brain: the visual system of the marmoset monkey. *Front Neural Circuits* 8:96
- Spinelli S, Pennanen L, Dettling AC, Feldon J, Higgins GA, Pryce CR (2004) Performance of the marmoset monkey on computerized tasks of attention and working memory. *Brain Res Cogn Brain Res* 19:123–137
- Stephan H, Baron G, Schwerdtfeger WK (1980) The brain of the common marmoset (*Callithrix jacchus*). A stereotaxic atlas. Springer, Berlin
- Suzuki W, Banno T, Miyakawa N, Abe H, Goda N, Ichinohe N (2015) Mirror neurons in a new world monkey, common marmoset. *Front Neurosci* 9:459
- Taha AA, Hanbury A (2015) Metrics for evaluating 3D medical image segmentation: analysis, selection, and tool. *BMC Med Imaging* 15:29
- Takemoto A, Miwa M, Koba R, Yamaguchi C, Suzuki H, Nakamura K (2015) Individual variability in visual discrimination and reversal learning performance in common marmosets. *Neurosci Res* 93:136–143
- Tardif SD, Smucny DA, Abbott DH, Mansfield K, Schultz-Darken N, Yamamoto ME (2003) Reproduction in captive common marmosets (*Callithrix jacchus*). *Comp Med* 53:364–368
- Thirion JP (1998) Image matching as a diffusion process: an analogy with Maxwell’s demons. *Med Image Anal* 2:243–260
- Toarmino CR, Yen CCC, Papoti D, Bock NA, Leopold DA, Miller CT, Silva AC (2017) Functional magnetic resonance imaging of auditory cortical fields in awake marmosets. *Neuroimage* 162:86–92
- Tomioka I, Ishibashi H, Minakawa EN et al (2017) Transgenic monkey model of the polyglutamine diseases recapitulating progressive neurological symptoms. *eNeuro* 4(2). <https://doi.org/10.1523/ENEURO.0250-16.2017>
- Tu TW, Turtzo LC, Williams RA, Lescher JD, Dean DD, Frank JA (2014) Imaging of spontaneous ventriculomegaly and vascular malformations in Wistar rats: implications for preclinical research. *J Neuropathol Exp Neurol* 73:1152–1165
- Tustison NJ, Avants BB, Cook PA, Zheng Y, Egan A, Yushkevich PA, Gee JC (2010) N4ITK: improved N3 bias correction. *IEEE Trans Med Imaging* 29:1310–1320
- Vercauteren T, Pennec X, Perchant A, Ayache N (2008) Symmetric log-domain diffeomorphic Registration: a demons-based approach. Medical image computing and computer-assisted intervention: MICCAI. *Int Conf Med Image Comput Comput Assist Interv* 11:754–761
- Vialard FX, Risser L, Rueckert D, Cotter CJ (2012a) Diffeomorphic 3D image registration via geodesic shooting using an efficient adjoint calculation. *Int J Comput* 97:229–241

- Vialard FX, Risser L, Rueckert D, Holm DD (2012b) Diffeomorphic atlas estimation using geodesic shooting on volumetric images. *Annl BMVA* 5:1–12
- Woodward A, Hashikawa T, Maeda M, Kaneko T, Hikishima K, Iriki A, Okano H, Yamaguchi Y (2018) The brain/MINDS 3D digital marmoset brain atlas. *Sci Data* 5:180009. <https://doi.org/10.1038/sdata.2018.9>
- Yeterian EH, Pandya DN, Tomaiuolo F, Petrides M (2012) The cortical connectivity of the prefrontal cortex in the monkey brain. *Cortex* 48:58–81
- Yokoyama C, Yamanaka H, Onoe K, Kawasaki A, Nagata H, Shirakami K, Doi H, Onoe H (2010) Mapping of serotonin transporters by positron emission tomography with [¹¹C]DASB in conscious common marmosets: comparison with rhesus monkeys. *Synapse* 64:594–601
- Yuasa S, Nakamura K, Kohsaka S (2010) Stereotaxic atlas of the marmoset brain. With immunohistochemical architecture and MR images. National Institute of Neuroscience (JP), Tokyo
- Yushkevich PA, Piven J, Hazlett HC, Smith RG, Ho S, Gee JC, Gerig G (2006) User-guided 3D active contour segmentation of anatomical structures: significantly improved efficiency and reliability. *Neuroimage* 31:1116–1128
- Zhu SC, Yuille A (1996) Region competition: unifying snakes, region growing, and Bayes/mdl for multiband image segmentation. *IEEE Trans Pattern Anal Mach Intell* 18:884–900

Publisher's Note Springer Nature remains neutral with regard to jurisdictional claims in published maps and institutional affiliations.

Affiliations

Laurent Risser¹ · Amirouche Sadoun² · Muriel Mescam² · Kuzma Strelnikov² · Sandra Lebreton¹ · Samuel Boucher² · Pascal Girard^{2,3} · Nathalie Vayssière² · Marcello G. P. Rosa^{4,5} · Caroline Fonta² 

Laurent Risser
lrisser@math.univ-toulouse.fr

Amirouche Sadoun
amirouche.sadoun@cnrs.fr

Muriel Mescam
muriel.mescam@cnrs.fr

Kuzma Strelnikov
kuzma.strelnikov@cnrs.fr

Sandra Lebreton
slebreton@math.univ-toulouse.fr

Samuel Boucher
samuel.boucher@inserm.fr

Pascal Girard
pascal.girard@cnrs.fr

Nathalie Vayssière
nathalie.vayssiere@cnrs.fr

¹ Institut de Mathématiques de Toulouse, UMR5219, Université de Toulouse, CNRS, UPS IMT, 31062 Toulouse Cedex 9, France

² Centre de recherche Cerveau et Cognition (CerCo), Université de Toulouse UPS, CNRS, UMR 5549, CHU Purpan, Pavillon Baudot, BP 25202, 31052 Toulouse Cedex 3, France

³ INSERM, Toulouse, France

⁴ Department of Physiology, Biomedicine Discovery Institute, Monash University, 26 Innovation Walk, Clayton, VIC 3800, Australia

⁵ Australian Research Council, Centre of Excellence for Integrative Brain Function, Monash University Node, Clayton, VIC 3800, Australia